

Structural and electronic properties of Na-B-H compounds at high pressure

Xing Li^{1,*}, Xiaohua Zhang^{1,*}, Aitor Bergara^{2,3,4}, Yong Liu¹, and Guochun Yang^{1,†}

¹State Key Laboratory of Metastable Materials Science & Technology and Key Laboratory for Microstructural Material Physics of Hebei Province, School of Science, Yanshan University, Qinhuangdao 066004, China

²Departamento de Física, Universidad del País Vasco-Euskal Herriko Unibertsitatea, UPV/EHU, 48080 Bilbao, Spain

³Donostia International Physics Center (DIPC), 20018 Donostia, Spain

⁴Centro de Física de Materiales CFM, Centro Mixto CSIC-UPV/EHU, 20018 Donostia, Spain

 (Received 22 August 2022; revised 11 October 2022; accepted 28 October 2022; published 9 November 2022)

Ternary hydrides are ideal candidates for high-temperature superconductivity. However, their electronic properties correlate strongly with the charge transfer between their consistent elements. In this work we propose nine Na-B-H compounds, which combines charge modulation between Na and B/H atoms with pressure, with unusual structural motifs and interesting electronic properties. In the metallic *Pmma* NaBH₃, with both ionic and covalent frameworks, formed by H atoms bonded to Na/B atoms, a low-frequency phonon dominated superconductivity is predicted with a T_c of 86.8 K, distinct from the high-frequency H-derived superconductivity associated with covalent H-based skeletons or H cages/sheets in superhydrides. Furthermore, in nonmetallic NaBH_{*n*} ($n = 1, 2,$ and 6) and *R-3m* NaBH₃, the B atom exhibits an *sp*³-hybridized feature analogous to the C atom, resulting in the formation of several alkanelike B-H motifs, such as a graphanelike layer and an ethane-shaped molecule. Our work presents an important step toward the understanding of metal borohydrides.

DOI: [10.1103/PhysRevB.106.174104](https://doi.org/10.1103/PhysRevB.106.174104)

I. INTRODUCTION

The search for high-temperature superconductors remains a hot topic in condensed matter physics. Since Ashcroft proposed that compressed H-rich hydrides have the potential to achieve high-temperature superconductivity [1], binary hydrides have been extensively explored [2–5]. Interestingly, two recent discoveries, covalent hydride H₃S (203 K at 155 GPa) [6,7] and clathrate hydride LaH₁₀ (260 K at 188 GPa) [8,9], have updated the record of the superconducting transition temperature (T_c), and have also revived the expectation of exploring room-temperature superconductors. Until now, many high- T_c superconductors have emerged in nonmetal and metal hydrides, e.g., the theoretically predicted 110 K for H₃Se at 250 GPa [10], 83 K for PH₃ at 200 GPa [11], 104 K for H₄Te at 170 GPa [12], 206 K for NaH₆ at 100 GPa [13], 263 K for MgH₆ at 300 GPa [14], 266 K for CaH₉ at 300 GPa [15], 234 K for HfH₁₀ at 250 GPa [16], 270 K for TbH₁₀ at 250 GPa [17], 303 K for YH₁₀ at 400 GPa [18], 329 K for ThH₁₈ at 350 GPa [19], and the experimentally confirmed 215 K for CaH₆ at 172 GPa [20], 262 K for YH₉ at 182 GPa [21], 115 K for CeH₉ at 95 GPa [22], 161 K for ThH₁₀ at 175 GPa [23], and others. Their common feature is that high-frequency phonons, contributed by H-based covalent skeletons and H cages/sheets, are responsible for the superconductivity. However, extremely high pressures are required to stabilize most of them, which restricts their immediate applications and remains a challenge [24].

Building on the success of binary hydrides, ternary hydrides have substantial prospects for achieving low-pressure high-temperature superconductivity, due to the unexpected “chemical precompression” and a set of potential crystal structures that could be stabilized [24,25]. Ma *et al.* proposed a design strategy for high- T_c superconductors by introducing additional electrons into the already known binary hydrides with abundant H₂ or H₃ molecules via metal doping; and successfully predicted a clathrate-type Li₂MgH₁₆ with an exciting T_c of 473 K at 250 GPa [26]. Additionally, room-temperature superconductivity of 556 K at 180 GPa has been recently observed in the La-B-N-H system [27], whereas the corresponding chemical compositions and crystal structures have not been resolved yet. So far, a plethora of ternary candidate hydrides with high- T_c values have been proposed, such as CaYH₁₂ (258 K at 200 GPa) [28], (La, Y)H₁₀ (253 K at 183 GPa) [29], LaBH₈ (156 K at 55 GPa) [30], and BaSiH₈ (71 K at 3 GPa) [31]. Interestingly, several types of isostructural hydrides present different stability regions, with diverse electronic and superconducting properties, as observed in *MC*₂H₈ ($M = \text{Na, K, Mg, Al, and Ga}$) [32] and *AX*H₈ ($A = \text{Sc, Ca, Y, Sr, La, Ba, and } X = \text{Be, B, Al}$) [24], indicating that the correct selection of constituent atoms is crucial.

For transition metal hydrides, their superconductivity depends not only on the number of electrons in *d/f* orbitals but also on the transferred charge from the transition metal atom to hydrogen [33,34]. If a large amount of *d/f* electrons contribute to states at the Fermi level (E_F), the hydrides usually show quite low T_c values, such as 0.3 K for Fe₂SH₃ at 173 GPa [35], 27.6 K for MgVH₆ at 150 GPa [36], and 52.9 K for ScYH₆ at 200 GPa [37]. On the other hand, if the transferred electrons from the transition metal atom are enough to

*These authors contributed equally to this work.

†Corresponding author: yanggc468@nenu.edu.cn

break the H_2 molecule, the hydrides present high T_c values due to the large H-dominated states at E_F and high-frequency H-derived vibrations. Consequently, the d/f electron modulation in transition metal hydrides plays a crucial role in realizing high-temperature superconductivity, becoming quite a complicated task.

In contrast to transition metals, alkali metals, with low atomic mass, simple s electronic channels, and strong electron-donating ability, have recently received considerable attention in the design of superconducting ternary hydrides. As it has been shown in Li-P-H [38,39] and Li-Si-H [40] systems, and in Li_2MgH_{16} , the incorporation of Li atoms as an electron dopant has become an effective route to improve the stability and superconductivity. Furthermore, after inserting Na/K atoms, the semiconducting CH_4 molecule becomes a metal and a superconductor at low pressure (≤ 50 GPa) [32]. Additionally, the insertion of alkali metals in the lightweight B-H system, which presents a maximum T_c of 37.3 K in $C2/c$ BH_2 below 300 GPa [41], can also greatly enhance the T_c up to ~ 100 K or more, as shown in Li_2BH_6 [42], and designed AB_2H_8 ($A = K, Rb, \text{ and } Cs$) [43,44]. In addition, various B-H motifs can be stabilized in Li-B-H compounds, including BH linear chains, BH_2 zigzag chains, BH_4 molecules, and BH_6 octahedra [42]. However, Na, the intermediate alkali metal between Li and K, with an unusual chemical identity [45], has been rarely explored in the design of ternary hydrides.

Our previous work has demonstrated that Na not only stabilizes distinctive boron cages in Na-B compounds, but also generates superconducting boron allotropes (e.g., $I4/mmm$ B_4 and Pm B_{17}) after the removal of Na atoms [46]. Recently, a distinct NaH_6 compound has been proposed by Zurek *et al.* [47], with a T_c comparable to the well-known CaH_6 [13], but with a different structure. These results give us a high motivation to explore the ternary Na-B-H system under pressure. In this work we perform a first-principles structure prediction study on the Na-B-H system at 100, 200, and 300 GPa, and identify several metallic and semiconducting structures. $Pm\bar{m}a$ $NaBH_3$ shows an interesting framework, and presents an unexpected low-frequency phonon-dominated superconductivity. $Pm\bar{m}n$ NaB_3H_3 , a compound derived from the insertion of Na atoms into $P6/mmm$ BH, presents a much higher T_c than the prototype BH. The unusual nonmetallic feature in Na-B-H compounds under pressure is associated with the presence of carbonlike structural units, such as alkane formed by B atoms. Overall, distinct chemical compositions, crystal structures, and electronic properties presented in the Na-B-H system will inject a great impetus into the exploration of new metal borohydrides.

II. COMPUTATIONAL DETAILS

The particle swarm optimization algorithm implemented in the CALYPSO code has been recognized as an important method to discover unknown compounds [3]. Here, the variable-composition structure search is performed for the Na-B-H system at selected pressures of 100, 200, and 300 GPa. The calculations of structural relaxations and electronic properties are carried out with the Vienna *ab initio* simulation package (VASP) code [48] based on the framework of density functional theory (DFT). The Perdew-Burke-Ernzerhof

(PBE) [49] generalized gradient approximation is chosen for the exchange-correlation functional. The projector augmented waves (PAWs) with $2s^22p^63s^1$, $2s^22p^1$, and $1s^1$ electrons are adopted as valence electrons for Na, B, and H atoms, respectively [50]. The kinetic cutoff energy of 700 eV and Monkhorst-Pack scheme with a k -point grid of $2\pi \times 0.03 \text{ \AA}^{-1}$ in the Brillouin zone are adopted to ensure an enthalpy convergence of less than 1 meV/atom. The electron localization function (ELF) [51] is used to describe both the electronic distribution and chemical bonding. Phonon calculations are performed by using the supercell finite displacement method in the PHONOPY code [52]. Superconducting properties are investigated via electron-phonon coupling (EPC) calculations implemented in the QUANTUM ESPRESSO package based on the density functional perturbation theory (DFPT) [53].

III. RESULTS AND DISCUSSION

Here, we extensively explore the low-enthalpy structures with stoichiometries of NaB_xH_y ($x = 1-8$, $y = 1-8$, 1-4 formula per simulation cell) and construct the ternary phase diagrams at 100, 200, and 300 GPa (Fig. 1). To accurately determine the thermodynamic stabilities of ternary Na-B-H compounds, their formation enthalpies are estimated relative to the already known stable structures of elemental solids [45,54-56] and binary compounds [41,46,47,57] (see the Supplemental Material for more details [58]). As shown in Fig. 1, eight chemical compositions are identified to be thermodynamically stable (e.g., $NaBH$, $NaBH_2$, $NaBH_3$, $NaBH_4$, $NaBH_6$, NaB_2H_2 , NaB_3H_3 , and NaB_4H_4), in which $Pm\bar{m}a$ $NaBH_4$ has been reported experimentally [59]. Additionally, a metastable Cm NaB_3H_4 compound, with a formation enthalpy of 19 meV/atom at 100 GPa, that is within the experimental synthesis (< 50 meV) [60], is also considered due to its interesting structure and properties, as will be discussed below. Only $NaBH_3$ experiences a structural phase transition from $R-3m$ to $Pm\bar{m}a$ with pressure. Additionally, we have also considered the already reported structural templates of K/Rb/Cs B_2H_8 [43,44] by replacing the alkali metal atoms with Na atoms. However, all of them have shown to be thermodynamically unstable as a consequence of their positive formation enthalpy. The absence of imaginary vibrational modes in phonon dispersion curves demonstrates that the predicted phases are dynamically stable (Fig. S1 [58]).

Based on the structural features and electronic properties (Fig. S2 [58]), the predicted Na-B-H compounds can be divided into two groups: metals ($NaBH_3$ with $Pm\bar{m}a$ symmetry, NaB_2H_2 , NaB_3H_3 , and NaB_4H_4) and semiconductors ($NaBH$, $NaBH_2$, $NaBH_3$ with $R-3m$ symmetry, $NaBH_6$, and NaB_3H_4).

For metallic phases, in $Pm\bar{m}a$ $NaBH_3$ [Fig. 2(a)], B atoms can coordinate with four H atoms (BH_4), and H atoms have two nonequivalent sites, labeled as H1 and H2 [Fig. 3(a)]. Note that the neighboring H1 atoms are paired with each other via a weak covalent bond, however the H2 atoms do not get paired. Interestingly, the BH_4 units are interconnected by sharing H1-H1 pairs and H2 atoms in the ac plane, and B-B bonds along the b axis, forming a channel-type covalent B-H framework [Fig. 2(a)]. Na atoms are located in the channel, and coordinate with 12 H atoms, resulting in a nested ionic

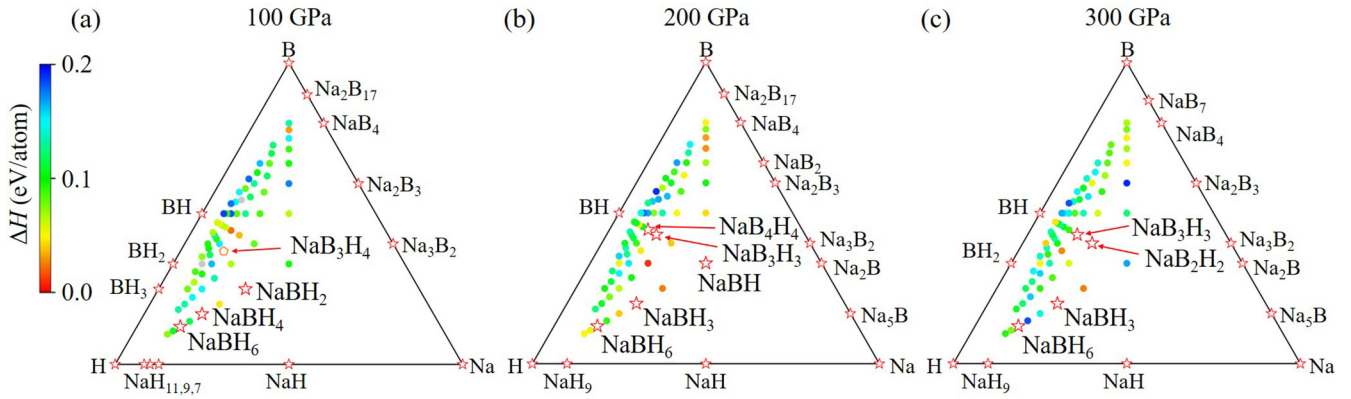


FIG. 1. Convex hulls of the Na-B-H system derived from the calculated formation enthalpies (ΔH) relative to stable elemental solids and binary compounds at (a) 100 GPa, (b) 200 GPa, and (c) 300 GPa. All stable compositions are represented by five-pointed stars, and a metastable compound is represented with a pentagon, whereas the colored dots denote the magnitude of the relative ΔH of the thermodynamic unstable phases.

network in the B-H framework [Fig. 2(a)]. Therefore, both the covalent B-H/B bonds and ionic Na-H ones are responsible for the structural stability.

On the other hand, the B/H ratio in the other three metallic phases is the same, and their stoichiometries can be written as $\text{Na}(\text{BH})_n$ ($n = 2, 3$, and 4). Moreover, their structural features are also similar [Figs. 2(b)–2(d)]. Specifically, each B atom is covalently bonded to a H atom. Meanwhile, all B atoms aggregate into wrinkled layers in the ab plane, with a hypercoordination characteristic, as a result of the electron deficiency attributed to B [69]. Accordingly, as observed in $Ibam$ BH, corrugated B-H layers are formed [57]. Na atoms are embedded between the B-H layers via ionic Na-H interaction; as a consequence, along the c axis $\text{Na}(\text{BH})_n$ exhibit a staggered distribution of ionic Na-H layers with covalent B-H ones (Fig. S3 [58]).

Among the four metallic compounds (Fig. S2), NaBH_3 , with a unique structural framework and the highest H content, attracts our attention to explore its electronic properties. The calculated projected density of states (PDOS) reveals that its metallicity is mainly derived from the B $2s/2p$, H1 $1s$, and H2 $1s$ states [Fig. 3(b)]. Moreover, these electronic states form several steep bands along the X - Γ , Z - T - Y , and U - R directions, and an electron pocket around the S point near the Fermi energy (E_F) [Fig. 3(c)], reflecting a large electronic DOS, which might enhance its electron-phonon coupling (EPC) [70].

Then we have investigated the superconducting properties of $Pmma$ NaBH_3 . The calculated EPC parameter λ is 1.25 at 300 GPa [Fig. 3(d)], which is significantly higher than 0.6 for $C2/c$ BH_2 at 250 GPa and slightly lower than 1.49 for $Pm\bar{3}m$ NaH_6 at 200 GPa [13,41]. Combining the Eliashberg spectral function $\alpha^2F(\omega)$ and phonon density of states (PHDOS), we conclude that the low-frequency vibrations (below 35 THz) contribute 72% to the total λ , whereas the medium-frequency vibrations associated to H1 and H2 atoms (35–76 THz) and the high-frequency vibrations from H1 atoms (76–114 THz) contribute 23% and 5%, respectively [Fig. 3(d)]. The fact that the contribution of H1 at high frequencies is greater than that of H2 can be attributed to the stronger binding strength of B-H1 than B-H2 [Fig. 3(a)]. Based on the phonon dispersion curves with λ weights, the strong EPC in the range 0–35 THz is mainly related to the phonon softening of acoustic branches at the X point and along the X - Γ direction [Fig. 3(e)], which can be associated to the Fermi surface nesting, as supported by the sharp peaks in the Fermi surface nesting function $\xi(Q)$ [Fig. 3(f)] [71]. Therefore, the superconductivity of $Pmma$ NaBH_3 originates mainly from the coupling of B $2s/2p$ and H $1s$ electrons with the lattice vibration modes at low frequencies, which contrasts with the well-known H-derived high-frequency dominated superconductivity in superhydrides (e.g., H_3S , LaH_{10} , and $\text{Li}_2\text{MgH}_{16}$) [6,8,26]. Since the Allen-Dynes modified McMillan equation is suitable for superconductors with $\lambda < 1.5$ [66], we use it to estimate the T_c of $Pmma$ NaBH_3 , and obtain a result of 86.8 K at 300 GPa with a typical Coulomb pseudopotential parameter of $\mu^* = 0.1$ [72,73], which is higher than 55 K of $P4/mmm$

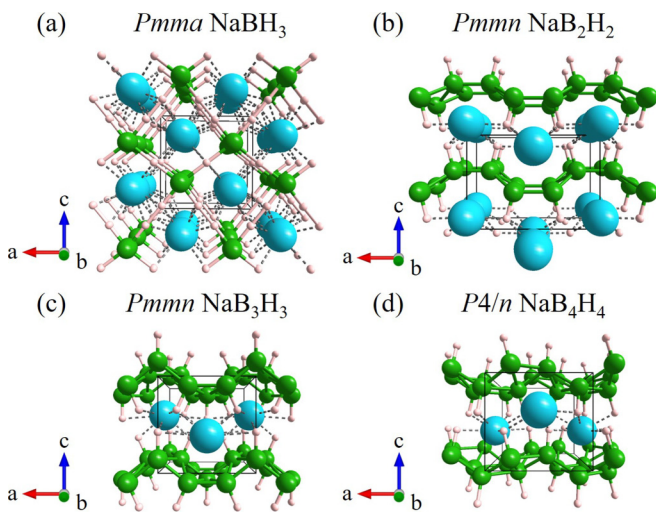


FIG. 2. The crystal structures of (a) $Pmma$ NaBH_3 at 300 GPa, (b) $Pmmn$ NaB_2H_2 at 300 GPa, (c) $Pmmn$ NaB_3H_3 at 200–300 GPa, and (d) $P4/n$ NaB_4H_4 at 200 GPa. The cyan, green, and pink spheres represent Na, B, and H atoms, respectively. To explicitly show the characters of chemical bonds, covalent bonds are shown in solid and bold lines, while ionic bonds are shown in dashed and narrow lines.

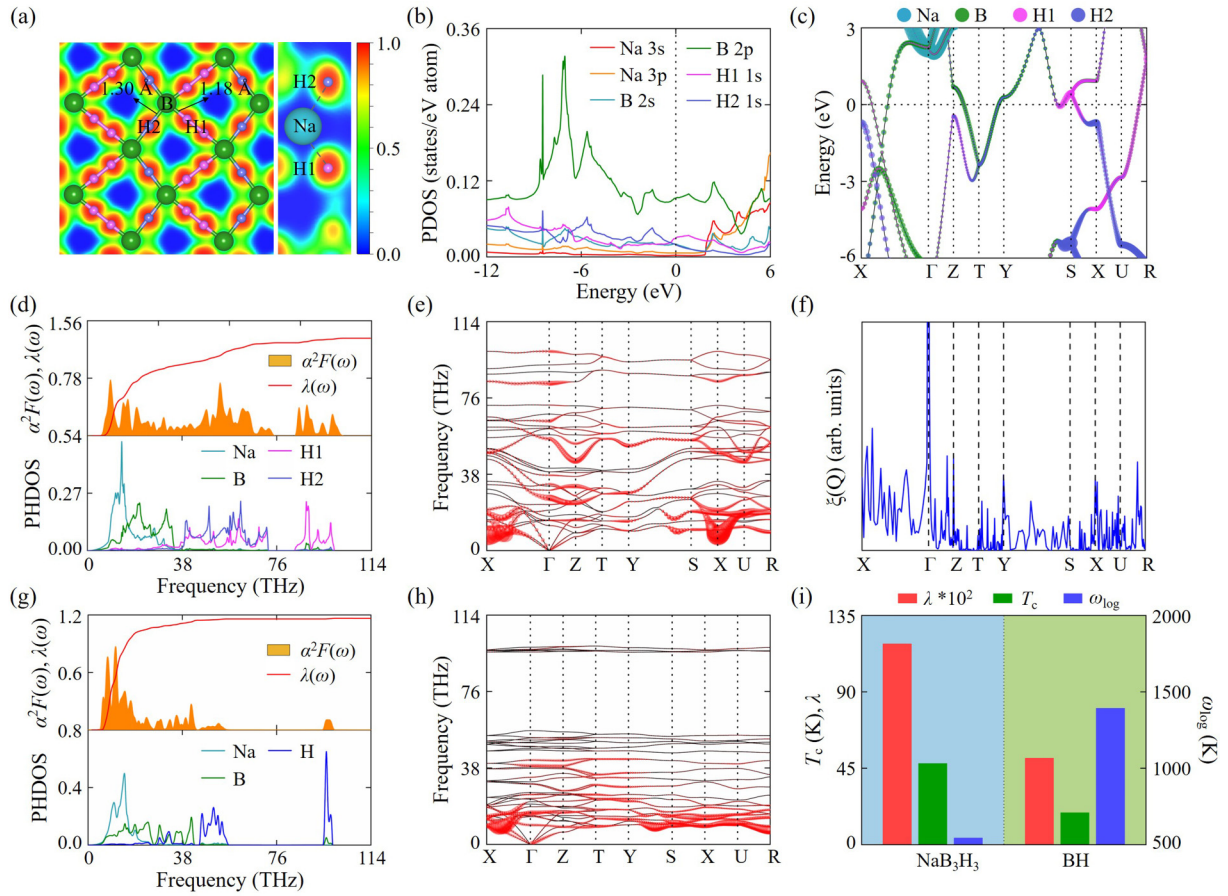


FIG. 3. (a) The ELF, (b) the PDOS, (c) the projected electronic band structure, (d) Eliashberg spectral function $\alpha^2F(\omega)$, EPC parameter $\lambda(\omega)$, and PHDOS, (e) the phonon dispersion curves (the magnitude of λ indicated by the thickness of the red curves), and (f) the Fermi surface nesting function $\xi(Q)$ of *Pnma* NaBH_3 at 300 GPa. (g) $\alpha^2F(\omega)$, $\lambda(\omega)$, PHDOS, and (h) the phonon dispersion curves with λ weights of *Pmnn* NaB_3H_3 at 200 GPa. (i) The T_c , λ , and the logarithmic average phonon frequency (ω_{\log}) values of *Pmnn* NaB_3H_3 and *P6/mmm* BH at 200 GPa.

NaAlH_8 and comparable to 89 K of *Pm* $\text{Ca}_2\text{B}_2\text{H}_{13}$ at 300 GPa, with a much higher H content [74,75].

On the other hand, an unexpected structural similarity of B-H layers (Fig. S4) with the same B/H ratio appears in *P6/mmm* BH and NaB_3H_3 , inspiring us to explore the role of Na atoms on the structure and physical properties. From a structural point of view, NaB_3H_3 can be obtained by inserting Na atoms into the B-H layers in *P6/mmm* BH and breaking the symmetric hydrogen bonds. In turn, we build a hypothetical $\text{Na}_0\text{B}_3\text{H}_3$ structure removing Na atoms in NaB_3H_3 . After structural relaxation, $\text{Na}_0\text{B}_3\text{H}_3$ actually converges into *P6/mmm* BH [57]. Then, we investigate the superconducting properties of NaB_3H_3 and *P6/mmm* BH at 200 GPa. The predicted λ value of NaB_3H_3 is 1.16, where phonon vibrations below 26.4 THz contribute 92% to the total λ [Fig. 3(g)], so that, similar to *P6/mmm* BH (the coupled B-H vibrations below 31.2 THz contribute 61.6% [57]), low-frequency phonon vibrations still play a crucial role in the EPC [Fig. 3(h)]. Comparing T_c , λ , and ω_{\log} values of NaB_3H_3 and *P6/mmm* BH, we conclude that, after inserting Na atoms, λ is doubled but ω_{\log} is significantly reduced [Fig. 3(i)]. The competition between λ and ω_{\log} causes the increase of T_c (47.8 K of NaB_3H_3 vs 18.8 K of BH), indicating that λ plays a dominant role in the evolution of T_c , which is inseparably associated

with the softening of low-frequency phonons [Fig. 3(h)]. As a consequence, the role of heavier Na atoms is to induce the low-frequency phonon softening.

In nonmetallic NaBH_y ($y = 1, 2, 3$, and 6) phases, B atoms are more likely than H atoms to get the electrons transferred by Na atoms, forming B-H morphologies analogous to alkanes, named as B-alkanes (Fig. 4). In detail, in *R-3m* NaBH [Fig. 4(a)], B atoms form wrinkled honeycomb layers in the *ab* plane. H atoms are bonded to B atoms on both sides of the honeycomb layer alternately, resulting in a graphanelike B-H motif, named B-graphane [76]. In *Pnma* NaBH_2 [Fig. 4(b)], B atoms form a saturated alkane-shaped BH_2 chain (B-alkane chain). In *R-3m* NaBH_3 [Fig. 4(c)], B and H atoms are in the ethane configuration (BH_3BH_3 , B-ethane), making it the first example in B-H systems, which contrasts with the double-bridging diborane molecule. In *R3m* NaBH_6 [Fig. 4(d)], there appear methanelike BH_4 molecules (B-methane), and H_2 molecules. Overall, a common feature in the semiconducting phases is that each B atom captures an electron donated by Na and behaves like a C atom (a Na/B ratio of 1:1), presenting a sp^3 hybridization and showing a tetrahedral coordination with the surrounding B and H atoms [42,77]. On the other hand, as the H content increases, the B-H motifs show a tendency to reduce the dimensionality,

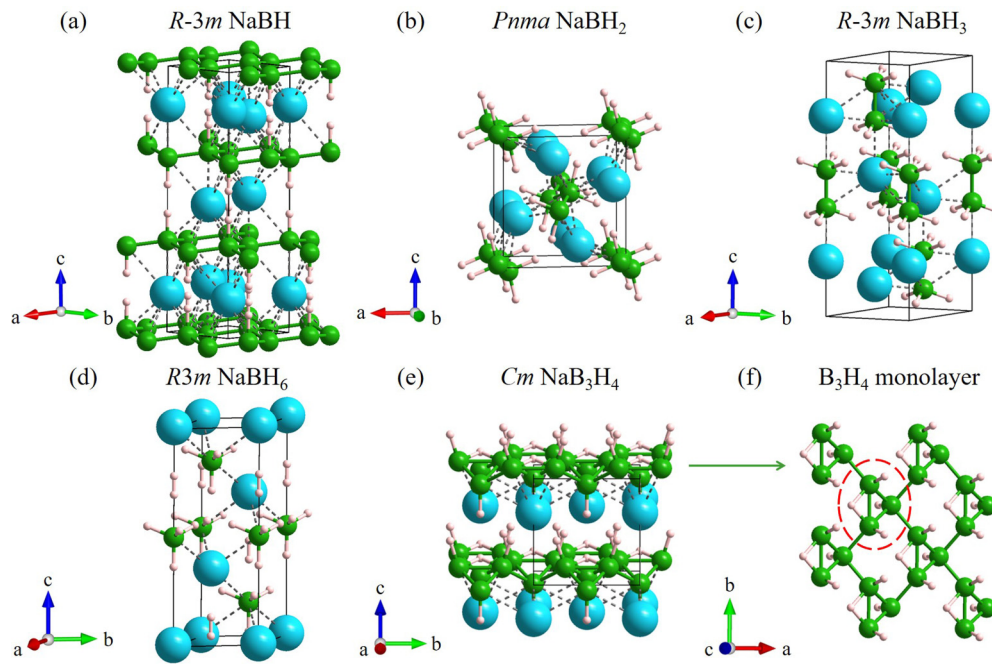


FIG. 4. The crystal structures of (a) $R-3m$ NaBH at 200 GPa, (b) $Pnma$ NaBH₂ at 100 GPa, (c) $R-3m$ NaBH₃ at 200 GPa, (d) $R3m$ NaBH₆ at 100–300 GPa, (e) Cm NaB₃H₄ at 100 GPa, and (f) the B₃H₄ monolayer of Cm NaB₃H₄ at 100 GPa. The cyan, green, and pink spheres represent Na, B, and H atoms, respectively.

from two-dimensional (2D) layers to 1D chains and then to 0D molecules.

Here, NaBH₆ is taken as an example to illustrate this feature. As can be seen in Fig. 5(a), the ELF isosurfaces of the BH₄ molecule in NaBH₆ and the CH₄ molecule show a similar

charge distribution. Additionally, the calculated PDOS reveals that B atoms are sp^3 hybridized [Fig. 5(b)]. In this case, all the constituent atoms can satisfy the octet rule, which leads to semiconducting properties. The same is true in NaBH_{*y*} ($y = 1, 2, \text{ and } 3$) compounds (Fig. S2). With increasing

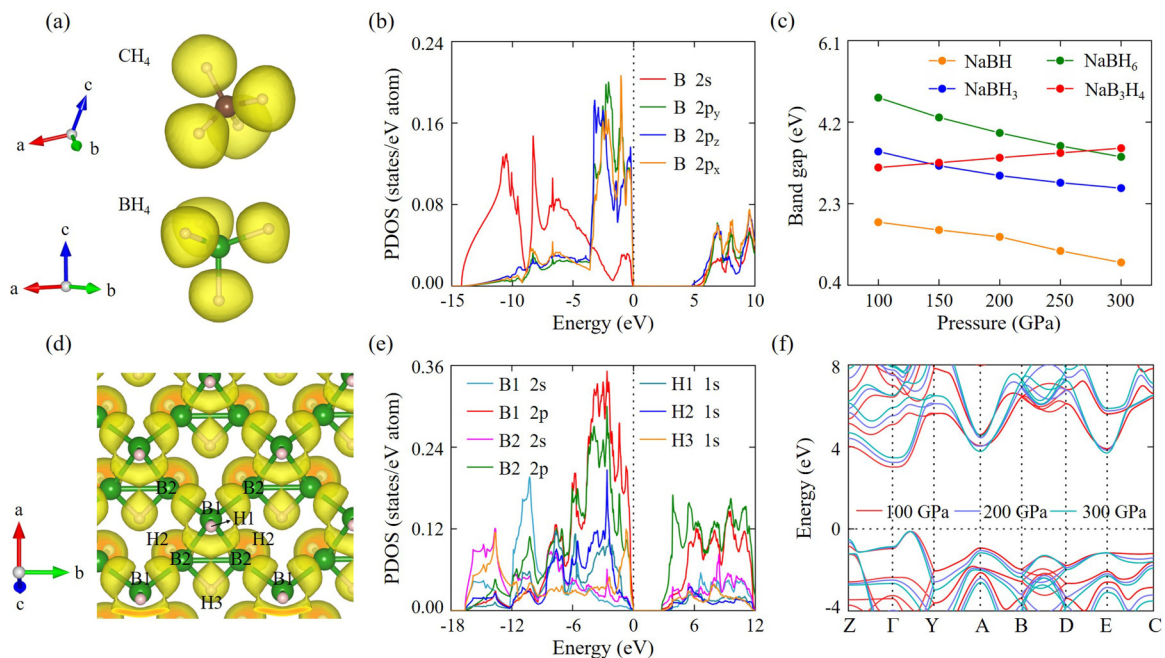


FIG. 5. (a) The ELF isosurfaces with a value of 0.75 of CH₄, and the BH₄ unit in NaBH₆. (b) The PDOS associated to the B atom in NaBH₆. (c) The band-gap evolution of NaBH, NaBH₃, NaBH₆, and NaB₃H₄ with pressure. (d) The ELF isosurfaces with a value of 0.75 in the B₃H₄ monolayer in Cm NaB₃H₄. (e) The PDOS associated to inequivalent B, and H atoms in NaB₃H₄. (f) The electronic band structures of NaB₃H₄ under different pressures.

pressure on these compounds, their band gaps gradually decrease [Fig. 5(c)], due to the decreasing interatomic distance which enhances the dispersion of the electronic bands. NaBH_2 is an exception, whose structure cannot be maintained at high pressure.

Compared with NaBH_y ($y = 1, 2, 3$, and 6), the small Na/B and B/H ratios (<1) in Cm NaB_3H_4 [Fig. 4(e)] drive a single-layer B-H formation [Fig. 4(f)], which consists of a building block of B_3H_4 , where B atoms are five coordinated [Fig. 5(d)]. Even if each Na atom in NaB_3H_4 can provide an electron, B atoms still do not have enough electrons to form two-center two-electron ($2c-2e$) covalent bonds. In other words, B atoms are in the multicenter bond form, which is a common feature of B atoms [69]. Based on the analysis of the solid state adaptive natural density partitioning (SSAdNDP) [78] and the ELF [Figs. S5 and 5(d)], B_3 and HB_2 triangles are in $3c-2e$ bonds, and B1-H1, B2-H2, and B1-B2 present $2c-2e$ bonds. The PDOS shows that NaB_3H_4 is also a semiconductor [Fig. 5(e)], which can be attributed to the separation of B_3H_4 units by saturated B1-B2 covalent bonds [79]. The band gap of NaB_3H_4 gradually increases with pressure in the range 100–300 GPa [Fig. 5(f)], which is in contrast with NaBH_y [$y = 1, 3$, and 6 ; Fig. 5(c)].

IV. CONCLUSIONS

In summary, we have systematically explored the energy landscape of the Na-B-H system at 100, 200, and 300 GPa using a first-principles structure prediction, and identified nine stable compounds, four metallic phases, and five semiconductors. In the metallic phases, the H-richest $Pmma$ NaBH_3 exhibits an exciting T_c of 86.8 K at 300 GPa, mainly originating from the contribution of low-frequency vibrations,

different from high-frequency H-dominated superconductivity in superhydrides. The low-frequency phonon dominated superconductivity is also confirmed in the comparative analysis of $Pm\bar{m}n$ NaB_3H_3 and $P6/mmm$ BH. On the other hand, a B atom captures the electron provided by each Na atom in NaBH_y ($y = 1, 2, 3$, and 6) to form diverse B-alkanes (e.g., B-graphane, B-alkane chain, B-ethane, and B-methane), behaving as a C atom, which is responsible for its semiconducting character. Our work is an important step to understand the role of alkali metals in the electronic and superconducting properties of borohydrides.

The data that support the findings of this study are available from the corresponding author upon reasonable request.

ACKNOWLEDGMENTS

The authors acknowledge funding from the Natural Science Foundation of China (Grants No. 21873017 and No. 21573037), the Innovation Capability Improvement Project of Hebei province (Grant No. 22567605H), the Natural Science Foundation of Hebei Province (Grant No. B2021203030), the Postdoctoral Science Foundation of China (Grant No. 2013M541283), and the Natural Science Foundation of Jilin Province (Grant No. 20190201231JC). This work was carried out at National Supercomputer Center in Tianjin, and the calculations were performed on TianHe-1 (A). A.B. acknowledges financial support from the Spanish Ministry of Science and Innovation (Grant No. PID2019-105488GB-I00) and the Department of Education, Universities and Research of the Basque Government and the University of the Basque Country (Grant No. IT1707-22).

The authors declare no competing financial interest.

-
- [1] N. W. Ashcroft, *Phys. Rev. Lett.* **21**, 1748 (1968).
 [2] A. R. Oganov, C. J. Pickard, Q. Zhu, and R. J. Needs, *Nat. Rev. Mater.* **4**, 331 (2019).
 [3] L. Zhang, Y. Wang, J. Lv, and Y. Ma, *Nat. Rev. Mater.* **2**, 17005 (2017).
 [4] C. J. Pickard, I. Errea, and M. I. Eremets, *Annu. Rev. Condens. Matter Phys.* **11**, 57 (2020).
 [5] G. Gao, J. Zhang, M. Li, L. Wang, R. T. Howie, E. Gregoryanz, V. V. Struzhkin, L. Wang, and S. T. John, *Mater. Today Phys.* **21**, 100546 (2021).
 [6] D. Duan, Y. Liu, F. Tian, D. Li, X. Huang, Z. Zhao, H. Yu, B. Liu, W. Tian, and T. Cui, *Sci. Rep.* **4**, 6968 (2014).
 [7] A. P. Drozdov, M. I. Eremets, I. A. Troyan, V. Ksenofontov, and S. I. Shylin, *Nature (London)* **525**, 73 (2015).
 [8] H. Liu, I. I. Naumov, R. Hoffmann, N. W. Ashcroft, and R. J. Hemley, *Proc. Natl. Acad. Sci. U.S.A.* **114**, 6990 (2017).
 [9] M. Somayazulu, M. Ahart, A. K. Mishra, Z. M. Geballe, M. Baldini, Y. Meng, V. V. Struzhkin, and R. J. Hemley, *Phys. Rev. Lett.* **122**, 027001 (2019).
 [10] S. Zhang, Y. Wang, J. Zhang, H. Liu, X. Zhong, H.-F. Song, G. Yang, L. Zhang, and Y. Ma, *Sci. Rep.* **5**, 15433 (2015).
 [11] H. Liu, Y. Li, G. Gao, J. S. Tse, and I. I. Naumov, *J. Phys. Chem. C* **120**, 3458 (2016).
 [12] X. Zhong, H. Wang, J. Zhang, H. Liu, S. Zhang, H.-F. Song, G. Yang, L. Zhang, and Y. Ma, *Phys. Rev. Lett.* **116**, 057002 (2016).
 [13] C.-H. Chen, A. Huang, C. Tsuei, and H.-T. Jeng, *New J. Phys.* **23**, 093007 (2021).
 [14] X. Feng, J. Zhang, G. Gao, H. Liu, and H. Wang, *RSC Adv.* **5**, 59292 (2015).
 [15] Z. Shao, D. Duan, Y. Ma, H. Yu, H. Song, H. Xie, D. Li, F. Tian, B. Liu, and T. Cui, *Inorg. Chem.* **58**, 2558 (2019).
 [16] H. Xie, Y. Yao, X. Feng, D. Duan, H. Song, Z. Zhang, S. Jiang, S. A. T. Redfern, V. Z. Kresin, C. J. Pickard *et al.*, *Phys. Rev. Lett.* **125**, 217001 (2020).
 [17] Y.-L. Hai, N. Lu, H.-L. Tian, M.-J. Jiang, W. Yang, W.-J. Li, X.-W. Yan, C. Zhang, X.-J. Chen, and G.-H. Zhong, *J. Phys. Chem. C* **125**, 3640 (2021).
 [18] F. Peng, Y. Sun, C. J. Pickard, R. J. Needs, Q. Wu, and Y. Ma, *Phys. Rev. Lett.* **119**, 107001 (2017).
 [19] X. Zhong, Y. Sun, T. Iitaka, M. Xu, H. Liu, R. J. Hemley, C. Chen, and Y. Ma, *J. Am. Chem. Soc.* **144**, 13394 (2022).
 [20] L. Ma, K. Wang, Y. Xie, X. Yang, Y. Wang, M. Zhou, H. Liu, X. Yu, Y. Zhao, H. Wang, G. Liu, and Y. Ma, *Phys. Rev. Lett.* **128**, 167001 (2022).

- [21] E. Snider, N. Dasenbrock-Gammon, R. McBride, X. Wang, N. Meyers, K. V. Lawler, E. Zurek, A. Salamat, and R. P. Dias, *Phys. Rev. Lett.* **126**, 117003 (2021).
- [22] W. Chen, D. V. Semenok, X. Huang, H. Shu, X. Li, D. Duan, T. Cui, and A. R. Oganov, *Phys. Rev. Lett.* **127**, 117001 (2021).
- [23] D. V. Semenok, A. G. Kvashnin, A. G. Ivanova, V. Svitlyk, V. Y. Fominski, A. V. Sadakov, O. A. Sobolevskiy, V. M. Pudalov, I. A. Troyan, and A. R. Oganov, *Mater. Today* **33**, 36 (2020).
- [24] Z. Zhang, T. Cui, M. J. Hutcheon, A. M. Shipley, H. Song, M. Du, V. Z. Kresin, D. Duan, C. J. Pickard, and Y. Yao, *Phys. Rev. Lett.* **128**, 047001 (2022).
- [25] X. Zhang, Y. Zhao, and G. Yang, *WIREs Comput. Mol. Sci.* **12**, e1582 (2022).
- [26] Y. Sun, J. Lv, Y. Xie, H. Liu, and Y. Ma, *Phys. Rev. Lett.* **123**, 097001 (2019).
- [27] A. D. Grockowiak, M. Ahart, T. Helm, W. A. Coniglio, R. Kumar, K. Glazyrin, G. Garbarino, Y. Meng, M. Oliff, V. Williams *et al.*, *Front. Electron. Mater.* **2**, 837651 (2022).
- [28] X. Liang, A. Bergara, L. Wang, B. Wen, Z. Zhao, X.-F. Zhou, J. He, G. Gao, and Y. Tian, *Phys. Rev. B* **99**, 100505(R) (2019).
- [29] D. V. Semenok, I. A. Troyan, A. G. Ivanova, A. G. Kvashnin, I. A. Kruglov, M. Hanfland, A. V. Sadakov, O. A. Sobolevskiy, K. S. Pervakov, and I. S. Lyubutin, *Mater. Today* **48**, 18 (2021).
- [30] X. Liang, A. Bergara, X. Wei, X. Song, L. Wang, R. Sun, H. Liu, R. J. Hemley, L. Wang, G. Gao *et al.*, *Phys. Rev. B* **104**, 134501 (2021).
- [31] R. Lucrezi, S. Di Cataldo, W. von der Linden, L. Boeri, and C. Heil, *npj Comput. Mater.* **8**, 1 (2022).
- [32] M.-J. Jiang, Y.-L. Hai, H.-L. Tian, H.-B. Ding, Y.-J. Feng, C.-L. Yang, X.-J. Chen, and G.-H. Zhong, *Phys. Rev. B* **105**, 104511 (2022).
- [33] D. V. Semenok, I. A. Kruglov, I. A. Savkin, A. G. Kvashnin, and A. R. Oganov, *Curr. Opin. Solid State Mater. Sci.* **24**, 100808 (2020).
- [34] X. Zhang, Y. Zhao, F. Li, and G. Yang, *Matter Radiat. Extremes* **6**, 068201 (2021).
- [35] S. Zhang, L. Zhu, H. Liu, and G. Yang, *Inorg. Chem.* **55**, 11434 (2016).
- [36] J. Zheng, W. Sun, X. Dou, A.-J. Mao, and C. Lu, *J. Phys. Chem. C* **125**, 3150 (2021).
- [37] Y. K. Wei, L. Q. Jia, Y. Y. Fang, L. J. Wang, Z. X. Qian, J. N. Yuan, G. Selvaraj, G. F. Ji, and D. Q. Wei, *Int. J. Quantum Chem.* **121**, e26459 (2021).
- [38] X. Li, Y. Xie, Y. Sun, P. Huang, H. Liu, C. Chen, and Y. Ma, *J. Phys. Chem. Lett.* **11**, 935 (2020).
- [39] Z. Shao, D. Duan, Y. Ma, H. Yu, H. Song, H. Xie, D. Li, F. Tian, B. Liu, and T. Cui, *npj Comput. Mater.* **5**, 104 (2019).
- [40] P. Zhang, Y. Sun, X. Li, J. Lv, and H. Liu, *Phys. Rev. B* **102**, 184103 (2020).
- [41] W.-H. Yang, W.-C. Lu, S.-D. Li, X.-Y. Xue, Q.-J. Zang, K.-M. Ho, and C.-Z. Wang, *Phys. Chem. Chem. Phys.* **21**, 5466 (2019).
- [42] C. Kokail, W. von der Linden, and L. Boeri, *Phys. Rev. Mater.* **1**, 074803 (2017).
- [43] M. Gao, X.-W. Yan, Z.-Y. Lu, and T. Xiang, *Phys. Rev. B* **104**, L100504 (2021).
- [44] S. Li, H. Wang, W. Sun, C. Lu, and F. Peng, *Phys. Rev. B* **105**, 224107 (2022).
- [45] Y. Ma, M. Eremets, A. R. Oganov, Y. Xie, I. Trojan, S. Medvedev, A. O. Lyakhov, M. Valle, and V. Prakapenka, *Nature (London)* **458**, 182 (2009).
- [46] S. Zhang, X. Du, J. Lin, A. Bergara, X. Chen, X. Liu, X. Zhang, and G. Yang, *Phys. Rev. B* **101**, 174507 (2020).
- [47] P. Baettig and E. Zurek, *Phys. Rev. Lett.* **106**, 237002 (2011).
- [48] G. Kresse and J. Furthmüller, *Phys. Rev. B* **54**, 11169 (1996).
- [49] J. P. Perdew, J. A. Chevary, S. H. Vosko, K. A. Jackson, M. R. Pederson, D. J. Singh, and C. Fiolhais, *Phys. Rev. B* **46**, 6671 (1992).
- [50] P. E. Blöchl, *Phys. Rev. B* **50**, 17953 (1994).
- [51] A. D. Becke and K. E. Edgecombe, *J. Chem. Phys.* **92**, 5397 (1990).
- [52] A. Togo, F. Oba, and I. Tanaka, *Phys. Rev. B* **78**, 134106 (2008).
- [53] P. Giannozzi, S. Baroni, N. Bonini, M. Calandra, R. Car, C. Cavazzoni, D. Ceresoli, G. L. Chiarotti, M. Cococcioni, I. Dabo *et al.*, *J. Phys. Condens. Matter* **21**, 395502 (2009).
- [54] Y. Li, Y. Wang, C. J. Pickard, R. J. Needs, Y. Wang, and Y. Ma, *Phys. Rev. Lett.* **114**, 125501 (2015).
- [55] A. R. Oganov, J. Chen, C. Gatti, Y. Ma, Y. Ma, C. W. Glass, Z. Liu, T. Yu, O. O. Kurakevych, and V. L. Solozhenko, *Nature (London)* **457**, 863 (2009).
- [56] C. J. Pickard and R. J. Needs, *Nat. Phys.* **3**, 473 (2007).
- [57] C.-H. Hu, A. R. Oganov, Q. Zhu, G.-R. Qian, G. Frapper, A. O. Lyakhov, and H.-Y. Zhou, *Phys. Rev. Lett.* **110**, 165504 (2013).
- [58] See Supplemental Material at <http://link.aps.org/supplemental/10.1103/PhysRevB.106.174104> for computational details, ELF and structural information of predicted Na-B-H phases, and the schematic diagram of the structural transition between BH and Pmmn NaB3H3, and the SSAdNDP chemical bonding analysis of the B3H4 layer, which includes Refs. [61–68].
- [59] Y. Filinchuk, A. V. Talyzin, D. Chernyshov, and V. Dmitriev, *Phys. Rev. B* **76**, 092104 (2007).
- [60] Y. Hinuma, T. Hatakeyama, Y. Kumagai, L. A. Burton, H. Sato, Y. Muraba, S. Iimura, H. Hiramatsu, I. Tanaka, H. Hosono *et al.*, *Nat. Commun.* **7**, 11962 (2016).
- [61] Y. Wang, J. Lv, L. Zhu, and Y. Ma, *Phys. Rev. B* **82**, 094116 (2010).
- [62] Y. Wang, J. Lv, L. Zhu, and Y. Ma, *Comput. Phys. Commun.* **183**, 2063 (2012).
- [63] J. P. Perdew, K. Burke, and M. Ernzerhof, *Phys. Rev. Lett.* **77**, 3865 (1996).
- [64] S. P. Ong, W. D. Richards, A. Jain, G. Hautier, M. Kocher, S. Cholia, D. Gunter, V. L. Chevrier, K. A. Persson, and G. Ceder, *Comput. Mater. Sci.* **68**, 314 (2013).
- [65] S. Baroni, S. de Gironcoli, A. Dal Corso, and P. Giannozzi, *Rev. Mod. Phys.* **73**, 515 (2001).
- [66] P. B. Allen and R. C. Dynes, *Phys. Rev. B* **12**, 905 (1975).
- [67] P. B. Allen and B. Mitrović, *Solid State Phys.* **37**, 1 (1983).
- [68] J. Carbotte, *Rev. Mod. Phys.* **62**, 1027 (1990).
- [69] B. Albert and H. Hillebrecht, *Angew. Chem., Int. Ed.* **48**, 8640 (2009).
- [70] A. Simon, *Angew. Chem., Int. Ed. Engl.* **36**, 1788 (1997).
- [71] W. Zhao, D. Duan, M. Du, X. Yao, Z. Huo, Q. Jiang, and T. Cui, *Phys. Rev. B* **106**, 014521 (2022).
- [72] P. Morel and P. W. Anderson, *Phys. Rev.* **125**, 1263 (1962).
- [73] A. Sanna, J. A. Flores-Livas, A. Davydov, G. Profeta, K. Dewhurst, S. Sharma, and E. K. U. Gross, *J. Phys. Soc. Jpn.* **87**, 041012 (2018).

- [74] H. Song, Z. Zhang, M. Du, Q. Jiang, D. Duan, and T. Cui, *Phys. Rev. B* **104**, 104509 (2021).
- [75] S. Di Cataldo, W. Von Der Linden, and L. Boeri, *Phys. Rev. B* **102**, 014516 (2020).
- [76] J. O. Sofo, A. S. Chaudhari, and G. D. Barber, *Phys. Rev. B* **75**, 153401 (2007).
- [77] F. Peng, M. Miao, H. Wang, Q. Li, and Y. Ma, *J. Am. Chem. Soc.* **134**, 18599 (2012).
- [78] D. Y. Zubarev and A. I. Boldyrev, *Phys. Chem. Chem. Phys.* **10**, 5207 (2008).
- [79] G. Guo, R. Wang, S. Luo, B. Ming, C. Wang, M. Zhang, Y. Zhang, and H. Yan, *Appl. Surf. Sci.* **518**, 146254 (2020).